

# Energy & Environmental Science

Accepted Manuscript



This is an *Accepted Manuscript*, which has been through the Royal Society of Chemistry peer review process and has been accepted for publication.

*Accepted Manuscripts* are published online shortly after acceptance, before technical editing, formatting and proof reading. Using this free service, authors can make their results available to the community, in citable form, before we publish the edited article. We will replace this *Accepted Manuscript* with the edited and formatted *Advance Article* as soon as it is available.

You can find more information about *Accepted Manuscripts* in the [Information for Authors](#).

Please note that technical editing may introduce minor changes to the text and/or graphics, which may alter content. The journal's standard [Terms & Conditions](#) and the [Ethical guidelines](#) still apply. In no event shall the Royal Society of Chemistry be held responsible for any errors or omissions in this *Accepted Manuscript* or any consequences arising from the use of any information it contains.

# Extraordinarily Efficient Photocatalytic Hydrogen Evolution in Water Using Semiconductor Nanorods Integrated With Crystalline Ni<sub>2</sub>P Cocatalyst

Zijun Sun, Huafei Zheng, Jingshi Li, Pingwu Du\*

Key Laboratory of Materials for Energy Conversion, Chinese Academy of Sciences, Department of Materials Science and Engineering, and the Collaborative Innovation Center of Chemistry for Energy Materials (*iChEM*), University of Science and Technology of China, 96 Jinzhai Road, Hefei, Anhui Province, 230026, P. R. China

\*Corresponding author: [dupingwu@ustc.edu.cn](mailto:dupingwu@ustc.edu.cn)

Tel/Fax: 86-551-63606207

**Abstract:** Photocatalytic hydrogen evolution *via* water splitting is an attractive scientific and technological goal to address the increasing global demand for clean energy and to reduce the climate change impact of CO<sub>2</sub> emission. Although tremendous efforts have been made, hydrogen production by a robust and highly efficient system driven by visible light still remains a significant challenge. Herein we report that nickel phosphide, as a cocatalyst to form a well-designed integrated photocatalyst with one-dimensional semiconductor nanorods, highly improves the efficiency and durability for photogeneration of hydrogen in water. The highest rate for hydrogen production reached  $\sim 1,200 \mu\text{mol}\cdot\text{h}^{-1}\cdot\text{mg}^{-1}$  based on the photocatalyst. The turnover number (TON) reached  $\sim 3,270,000$  in 90 hours with a turnover frequency (TOF) of 36,400 for Ni<sub>2</sub>P, and the apparent quantum yield was  $\sim 41\%$  at 450 nm. The photoinduced charge transfer process was further confirmed by steady-state photoluminescence spectra and time-resolved photoluminescence spectra. Such extraordinary performance of a noble-metal-free artificial photosynthetic hydrogen production system has, to our knowledge, not been reported to date.

**Broader context.** The world's energy supply in the future depends on innovative breakthroughs regarding the design of low-cost, durable and efficient systems for clean energy conversion and storage. The production of hydrogen through water splitting via electrolysis/photocatalysis seems a promising and appealing pathway. The current technology for photocatalytic water splitting relies on expensive noble metal-based catalysts, such as Pt, Ru, and Ir. The present study on water splitting for H<sub>2</sub> production describes a highly active, noble-metal-free, crystalline nickel phosphide as the cocatalyst on semiconductor nanorods for extraordinarily efficient H<sub>2</sub> production from water. The exceptional catalytic activity is probably contributed to fast charge separation between the nickel phosphide and the semiconductor nanorods.

## Introduction

Due to the increasing global energy demand and the climate change impact of CO<sub>2</sub> emission from energy production, finding an abundant and renewable energy alternative to fossil fuels has become one of the most significant challenges for human society.<sup>1-2</sup> Artificial photosynthesis (AP), which facilely converts solar energy into chemically stored energy, represents an intriguing approach to provide renewable energy.<sup>3-5</sup> The general design for AP systems is to produce hydrogen (H<sub>2</sub>) *via* photocatalytic water splitting using solar energy, including the water oxidation half-reaction to O<sub>2</sub> and the proton reduction half-reaction to H<sub>2</sub>.<sup>6</sup> For the H<sub>2</sub> evolution reaction (HER), the multi-component photocatalysts are usually composed of a photosensitizer and a cocatalyst, while an electron source is needed to allow only the reductive half-reaction to be studied.<sup>7</sup> A successful HER system will be coupled eventually with the oxidative side to achieve efficient overall water splitting. Cocatalysts loaded onto the photosensitizer can highly promote the photoexcited electron-hole pair separation, reduce the activation potentials for H<sub>2</sub> or O<sub>2</sub> evolution, and subsequently enhance the activities of the photocatalysts.<sup>8</sup> The reported catalysts for H<sub>2</sub> evolution are mostly made from the precious metals, such as platinum, so their scarcity and high cost hamper their practicality in applications. For this reason, the investigation of novel active catalysts made of inexpensive earth-abundant materials is highly desirable.

Recently, extensive studies have reported many abundant and low-cost materials to replace noble metal catalysts for H<sub>2</sub> evolution.<sup>9-10</sup> The conversion of protons to H<sub>2</sub> is actually an important biological process catalyzed by iron-based hydrogenases in nature.

Many efforts have focused on mimicking the hydrogenase enzymes,<sup>11-12</sup> and some of these have achieved very high TON and TOF for electrochemical hydrogen production.<sup>13-14</sup> Meanwhile, functional models of hydrogenases based on other earth-abundant elements have been rapidly developed, including nickel (Ni),<sup>15-18</sup> cobalt (Co),<sup>4-5,10,19-22</sup> molybdenum (Mo),<sup>23-27</sup> and tungsten (W).<sup>26,28</sup> Co-based cobaloximes have been reported as active electrocatalysts for H<sub>2</sub> evolution, with a highest turnover frequency (TOF) at ~295 s<sup>-1</sup>.<sup>29-31</sup> Impressively, DuBois and coworkers reported a series of efficient Ni-based molecular catalysts,<sup>32-33</sup> in which the highest reaction TOF has reached as high as 100,000 s<sup>-1</sup>.<sup>33</sup> Some of these electrocatalysts have been used in a homogeneous photocatalytic H<sub>2</sub> evolution system by combining them with a photosensitizer and electron donor, but doing so significantly decreases the catalytic efficiency (TOF <110 h<sup>-1</sup> and TON <9000 in 8 hours for Co,<sup>34</sup> TOF <18 h<sup>-1</sup> and TON <2700 in 150 hours for Ni<sup>35</sup>) and the stability is low (H<sub>2</sub> evolution generally ceases after 10 hours of irradiation). Co-dithiolene complexes have also been shown to yield a higher rate for photocatalytic H<sub>2</sub> production (TOF ~880 h<sup>-1</sup>).<sup>36</sup> Meanwhile, it has been demonstrated that heterogeneous catalysts are quite robust for light-driven HER with high efficiencies. Sulfides of transition metals are well studied as cocatalysts in photocatalytic H<sub>2</sub> production. One example of MoS<sub>2</sub>/CdS system has shown an H<sub>2</sub> evolution rate of ~5,000 μmol · h<sup>-1</sup> · g<sup>-1</sup> and TOF of ~162 h<sup>-1</sup>.<sup>37</sup> Eisenberg and coworkers have reported an H<sub>2</sub> evolution system that is driven by visible light and contains CdSe quantum dots as the photosensitizer and Ni-DHLA as the cocatalyst, which showed extremely high efficiency (TON ~600,000 in 110 hours for Ni, TOF ~7,000 moles of

H<sub>2</sub> per mole of catalyst per hour) and longevity (no significant decrease for >2 weeks).<sup>38</sup>

The Wu group demonstrated that an artificial Co-based catalyst also has great efficiency (TON ~59,600 in 70 hours for Co, rate of H<sub>2</sub> evolution ~25,000 μmol·h<sup>-1</sup>·g<sup>-1</sup>).<sup>39</sup> Other cocatalysts, such as Ni,<sup>40</sup> NiO,<sup>41</sup> Ni(OH)<sub>2</sub>,<sup>42</sup> NiS,<sup>43</sup> are also studied as cocatalysts for photocatalysis but they have much lower activities and stability than the above two systems.

On the other hand, the photocatalytic activity is also affected by the morphology of a catalyst. One-dimensional nanorod morphologies show the advantages of large surface area with high length-to-diameter ratios and fast charge separation efficiencies with short radial distances, which probably help improve the activity of photocatalytic H<sub>2</sub> evolution.<sup>44-46</sup> Herein, we report the integrated heterostructure by tightly anchoring crystalline nickel phosphide (Ni<sub>2</sub>P) as the cocatalyst onto one-dimensional CdS nanorods (NRs) for photocatalytic H<sub>2</sub> evolution in water under visible light (Figure 1). The system shows extraordinarily high activity and great stability. Under optimal conditions, the highest rate observed for H<sub>2</sub> evolution was ~1,200 μmol·h<sup>-1</sup>·mg<sup>-1</sup> based on the photocatalyst. The TON reached ~3,270,000 in 90 hours with a TOF of 36,400 for Ni<sub>2</sub>P and the apparent quantum yield was ~41% at 450 nm in 8 hours. The catalytic activity with regard to TOF, TON, and the H<sub>2</sub> evolution rate, to the best of our knowledge, is the highest in a noble-metal-free artificial photocatalytic H<sub>2</sub> production system.

## Results and discussion

**Preparation of the Ni<sub>2</sub>P/CdS photocatalyst composites.** To prepare Ni<sub>2</sub>P/CdS NRs photocatalyst, we first synthesized CdS NRs by a solvothermal reaction of CdCl<sub>2</sub> · 2.5 H<sub>2</sub>O and NH<sub>2</sub>CSNH<sub>2</sub> at 160 °C.<sup>47</sup> After filtration and washing, the as-synthesized CdS NRs were added into a mixture of Ni(NO<sub>3</sub>)<sub>2</sub> · 6H<sub>2</sub>O and yellow phosphorous in ethylenediamine for another solvothermal treatment at 140 °C. The resulting Ni<sub>2</sub>P/CdS NRs were obtained after centrifugation, followed by washing three times each with benzene, ethanol and distilled water. The Ni<sub>2</sub>P/CdS NRs catalysts with different weight ratios of Ni<sub>2</sub>P were synthesized by adjusting the initial amount of Ni(NO<sub>3</sub>)<sub>2</sub> · 6H<sub>2</sub>O and yellow phosphorous. For comparison, Ni<sub>2</sub>P was also prepared using the same method in the absence of CdS NRs. A detailed description of the experimental method is given in the methods section below.

**Visible light-driven H<sub>2</sub> evolution.** Figure 2a shows the H<sub>2</sub> evolution rate of Ni<sub>2</sub>P/CdS NRs photocatalysts with loading of different amounts of Ni<sub>2</sub>P. Pure CdS NRs and Ni<sub>2</sub>P were used for comparison. No appreciable H<sub>2</sub> was observed when Ni<sub>2</sub>P alone was used under visible light irradiation ( $\lambda > 420$  nm), revealing that Ni<sub>2</sub>P is not an active photocatalyst. CdS NRs themselves showed photocatalytic activity for H<sub>2</sub> evolution but not with an efficient rate ( $\sim 25$   $\mu\text{mol}\cdot\text{h}^{-1}\cdot\text{mg}^{-1}$ ). Moreover, the photocatalytic H<sub>2</sub> evolution activity of CdS NRs with solvothermal treatment was also examined and the result showed a similar rate ( $\sim 25.3$   $\mu\text{mol}\cdot\text{h}^{-1}\cdot\text{mg}^{-1}$ ) as that of CdS without solvothermal treatment, indicating that further solvothermal method did not significantly change the CdS NRs activity (Figure S1). In contrast, with only 0.25 wt % of Ni<sub>2</sub>P loaded on CdS NRs, the Ni<sub>2</sub>P/CdS NRs photocatalyst exhibited a highly enhanced H<sub>2</sub> evolution rate of

$\sim 225 \mu\text{mol}\cdot\text{h}^{-1}\cdot\text{mg}^{-1}$ . With increasing amount of  $\text{Ni}_2\text{P}$  loaded on CdS NRs, the  $\text{H}_2$  evolution rate increased. The highest photocatalytic activity was achieved with 0.5 wt %  $\text{Ni}_2\text{P}$  loading, providing an extraordinary  $\text{H}_2$  evolution rate of  $\sim 553 \mu\text{mol}\cdot\text{h}^{-1}\cdot\text{mg}^{-1}$ , which is about 22 times higher than that of CdS NRs alone. The reaction system produced a large amount of gas bubbles in a cuvette, observable by the naked eye (Movie S1). Further increasing the content of  $\text{Ni}_2\text{P}$ , however, resulted in a decrease of the photocatalytic activity and the  $\text{H}_2$  evolution rate was reduced to  $\sim 270 \mu\text{mol}\cdot\text{h}^{-1}\cdot\text{mg}^{-1}$  with 10 wt %  $\text{Ni}_2\text{P}$  loading. Since platinum is a well-known active catalyst for HER and it has been used to enable remarkable performance for hydrogen production, we also measured the hydrogen evolution properties of 0.5 wt % Pt/CdS NRs for comparison under exactly the same conditions (Figure S2). The  $\text{H}_2$  evolution rate was  $\sim 167 \mu\text{mol}\cdot\text{h}^{-1}\cdot\text{mg}^{-1}$ , which is much lower than that of 0.5 wt %  $\text{Ni}_2\text{P}/\text{CdS}$  NRs, indicating that  $\text{Ni}_2\text{P}$  is an excellent cocatalyst for promoting highly efficient photocatalytic hydrogen production in the present system. Besides, the photocatalytic activities of CdS NRs, CdS nanoparticles (CdS NPs), 0.5 wt%  $\text{Ni}_2\text{P}/\text{CdS}$  NRs, and 0.5 wt%  $\text{Ni}_2\text{P}/\text{CdS}$  NPs have also measured, as shown in Figure S3. The CdS NRs show a higher photocatalytic  $\text{H}_2$  evolution rate than CdS NPs under the same conditions and 0.5 wt%  $\text{Ni}_2\text{P}/\text{CdS}$  NRs also show much higher photocatalytic activity than 0.5 wt%  $\text{Ni}_2\text{P}/\text{CdS}$  NPs, demonstrating that one-dimensional structure probably have better photocatalytic activity than bulk structure under our present conditions.

Figure 2b shows the influence of electron donors on photocatalytic activity of  $\text{Ni}_2\text{P}/\text{CdS}$  NRs for  $\text{H}_2$  production. With increasing concentration of the sacrificial

electron donors ( $\text{Na}_2\text{S}$  and  $\text{Na}_2\text{SO}_3$ ), the photocatalytic activity rapidly increased. The reaction reached a maximum rate for  $\text{H}_2$  evolution at  $\sim 553 \mu\text{mol}\cdot\text{h}^{-1}\cdot\text{mg}^{-1}$  in the presence of 0.75 M  $\text{Na}_2\text{S}$  and 1.05 M  $\text{Na}_2\text{SO}_3$ . The rate slightly decreased and stayed at  $\sim 530 \mu\text{mol}\cdot\text{h}^{-1}\cdot\text{mg}^{-1}$  when the concentrations of the electron donors further increased, indicating that the electron donors could not further improve the photocatalytic activity after an optimal concentration. When the concentration of  $\text{Na}_2\text{S}$  and  $\text{Na}_2\text{SO}_3$  reached 2 M and 2.8 M respectively, the reaction solution was oversaturated with obviously undissolved  $\text{Na}_2\text{SO}_3$ . Under this concentration, the  $\text{H}_2$  evolution rate decreased to  $\sim 390 \mu\text{mol}\cdot\text{h}^{-1}\cdot\text{mg}^{-1}$ , probably due to the loss of light energy blocked by the undissolved  $\text{Na}_2\text{SO}_3$  particles.

**$\text{H}_2$  evolution stability.** Figure 3a shows the stability of photocatalytic  $\text{H}_2$  evolution using 0.5 wt %  $\text{Ni}_2\text{P}/\text{CdS}$  NRs catalyst and the amount of  $\text{H}_2$  was measured by gas chromatography (GC). After 90 hours of visible light irradiation ( $\lambda > 420 \text{ nm}$ ) under appropriate conditions (1.0 mg 0.5 wt %  $\text{Ni}_2\text{P}/\text{CdS}$  NRs photocatalyst, 1.25 M  $\text{Na}_2\text{S}$ , and 1.75 M  $\text{Na}_2\text{SO}_3$  dispersed in 50 mL deionized water), the  $\text{H}_2$  evolution rate had no significant decrease. More than 100 mmol  $\text{H}_2$  was produced during the course of 90 hours of the  $\text{H}_2$  evolution experiment. The highest  $\text{H}_2$  evolution rate reached  $\sim 1,200 \mu\text{mol}\cdot\text{h}^{-1}\cdot\text{mg}^{-1}$  based on the photocatalyst during the period of irradiation, indicating that the present artificial photosynthetic  $\text{H}_2$  production system is quite robust and highly efficient under visible light irradiation. When the evolved  $\text{H}_2$  gas was produced through water via a long stainless steel needle ( $\sim 20 \text{ cm}$ ), gas bubbles were clearly observed at an almost constant rate of  $\sim 1.8 \text{ bubbles}\cdot\text{s}^{-1}$  and the average diameter of the bubbles is

~2 mm (Movie S2, 1.0 mg 0.5 wt % Ni<sub>2</sub>P/CdS NRs photocatalyst, 1.25 M Na<sub>2</sub>S, and 1.75 M Na<sub>2</sub>SO<sub>3</sub> dispersed in 50 mL deionized water). This corresponds to a hydrogen evolution rate at ~27 mL per hour, which is consistent with the result measured by GC. This system has achieved an optimal TON of 3,270,000 and TOF of 36,400 for Ni<sub>2</sub>P in 90 hours under visible light illumination. To the best of our knowledge, these TON and TOF numbers are the highest values for a visible light-driven H<sub>2</sub> production system in water.

Further experiments were performed to confirm the photocatalytic stability of the Ni<sub>2</sub>P/CdS NRs under visible light irradiation. The reaction system was evacuated every 2 hours and the process was carried out for repeated cycles. As shown in Figure 3b, there was no significant decrease in H<sub>2</sub> evolution through each cycle. The Ni<sub>2</sub>P/CdS NRs photocatalyst showed excellent stability and maintained a similar photocatalytic activity for more than 12 hours, indicating good stability of this material for H<sub>2</sub> evolution.

More interestingly, the present reaction system shows great photocatalytic activity under aerobic conditions. When the solution was exposed to air, a large number of bubbles were still rapidly generated from aqueous solution under visible light illumination (Movie S3). Figure 3c shows the H<sub>2</sub> evolution plot of the Ni<sub>2</sub>P/CdS NRs photocatalyst in air, demonstrating an H<sub>2</sub> evolution rate of ~255 μmol·h<sup>-1</sup>·mg<sup>-1</sup>. Although the H<sub>2</sub> evolution rate under aerobic conditions is lower than that under inert atmosphere which may be due to the backward reaction of H<sub>2</sub> and O<sub>2</sub> to form H<sub>2</sub>O on the photocatalyst surface,<sup>48-50</sup> it is still much higher than that of CdS NRs without a

Ni<sub>2</sub>P cocatalyst.

**Quantum yield.** The apparent quantum yield ( $\phi$ ) for H<sub>2</sub> evolution was determined for the photocatalytic system containing 1.0 mg 0.5 wt % Ni<sub>2</sub>P/CdS NRs, 0.75 M Na<sub>2</sub>S, and 1.05 M Na<sub>2</sub>SO<sub>3</sub> in 20 mL deionized water. The solution was irradiated by 450 nm ( $\pm 5$  nm) visible light irradiation and the result is shown in Figure 3d. One molecule of H<sub>2</sub> is assumed to be generated by the absorption of two photons. The H<sub>2</sub> evolution rate was  $\sim 140 \mu\text{mol}\cdot\text{h}^{-1}\cdot\text{mg}^{-1}$  with  $\phi > 37\%$  after 2 hours and the value was lower in the first hour ( $\sim 25\%$ ), which may be due to an induction period at the early stages and the dissolved H<sub>2</sub> in the solution.<sup>38-39</sup> The highest  $\phi$  reached  $\sim 41\%$  after 6 hours, which is higher than recently reported Ni/CdS and Ni/CdSe systems but lower than a reported PdS/CdS/Pt system based on dual cocatalysts.<sup>51</sup> Efficient conversion of visible light energy presumably suggests that the present Ni<sub>2</sub>P/CdS NRs catalyst is highly active for electron-hole pair generation and separation.

**Morphologies and crystalline properties.** The surface morphologies of Ni<sub>2</sub>P/CdS NRs are illustrated in Figure 4. SEM images (Figure 4a) show that Ni<sub>2</sub>P/CdS NRs have an average diameter of  $\sim 55$  nm, length of 1-3  $\mu\text{m}$ , and surface area of  $\sim 25.5 \text{ m}^2 \text{ g}^{-1}$  from BET (Figure S4). There are no appreciable changes when the loading ratio of Ni<sub>2</sub>P is increased (Figure S5). Besides, the SEM images of CdS NPs were measured, presenting an average diameter of  $\sim 100$  nm (Figure S6a). TEM images show consistent average diameter and length of Ni<sub>2</sub>P/CdS NRs (Figure 4b). In addition, with increasing ratio of Ni<sub>2</sub>P, tiny nanoparticles with sizes of  $\sim 10$  nm gradually appear and are tightly bound onto the nanorods. Supplementary Figure S7a shows an image of pure CdS NRs with

no nanoparticles on the nanorods, indicating these nanoparticles in Supplementary Figure S7b-S7e could be Ni<sub>2</sub>P. Besides, the EDX data (Figure 4c) show the existence of Ni, P, Cd, and S, implying Ni<sub>2</sub>P material was successfully loaded on the CdS NRs.

The XRD patterns (Figure 4d) show appreciable sharp diffraction peaks, indicating high quality of crystallinity in all the photocatalyst samples. The diffraction patterns of CdS NRs were indexed to the hexagonal phase (PDF#77-2306), and Ni<sub>2</sub>P were also indexed to the hexagonal phase (PDF#03-0953). When Ni<sub>2</sub>P (< 10 wt %) was loaded on CdS NRs, no obvious diffraction peaks belonging to Ni<sub>2</sub>P were observed and all reflections showed no significant difference from the CdS NRs, probably due to too strong diffraction peaks of CdS NRs and the relatively small amount of Ni<sub>2</sub>P dispersed on the surface of the CdS NRs. Therefore, we prepared an 80 wt % Ni<sub>2</sub>P/CdS NRs sample for XRD. The data clearly show the characteristic diffraction peaks of Ni<sub>2</sub>P and CdS, confirming that Ni<sub>2</sub>P has been successfully loaded on the CdS NRs. In addition, the XRD pattern of CdS NPs is showed in Figure S6b, which can be also indexed to the hexagonal phase of CdS (PDF#77-2306).

In order to clearly visualize the structure of Ni<sub>2</sub>P and CdS, HRTEM was used to investigate 0.5 wt % Ni<sub>2</sub>P/CdS NRs, as shown in Figure 4e-4f and Supplementary Figure S8. The HRTEM images in Figure 4e and Supplementary Figure S8a-8b confirm that Ni<sub>2</sub>P cocatalyst nanoparticles are anchored on the surface of CdS NRs to form a Ni<sub>2</sub>P-CdS junction. High-magnification HRTEM images (Figure 4f and Figure S8c) exhibit lattice spacing of approximately 2.2 Å and 3.1 Å, corresponding to the (111) plane of hexagonal Ni<sub>2</sub>P and (101) plane of hexagonal CdS, respectively. A more

detailed observation of the images indicates that Ni<sub>2</sub>P is tightly deposited on the surface of the CdS NRs. On the basis of selected-area electron diffraction (SAED) analysis (Figure S8d), these nanorods were consistently found to be single-crystalline.

**XPS and ICP-AES study.** The presence and content of Ni<sub>2</sub>P on the surface of the CdS NRs was further studied by XPS (Figure S9) and ICP-AES measurements. The XPS survey spectrum shows the existence of Cd, S, Ni, and P elements, as well as C as the reference and O impurities from absorbed gaseous molecules. The high resolution XPS spectrum of Cd 3d shows two peaks at Cd 3d<sub>5/2</sub> (404.9 eV) and Cd 3d<sub>3/2</sub> (411.6 eV), together with the S 2p<sub>3/2</sub> (160.9 eV) and S 2p<sub>1/2</sub> (162.1 eV), which is the typical character of CdS.<sup>42,52</sup> After visible light irradiation, the XPS spectra of Cd 3d and S 2p show no significant changes, indicating that CdS is stable and the system did not produce NiS or S-doped Ni<sub>2</sub>P during the irradiation. The high resolution XPS spectrum of P 2p shows one peak at 133.3 eV, probably corresponding to phosphate species bonded on the catalyst surface during solvothermal synthesis under the phosphorus-rich conditions. After irradiation, the peak intensity decreased, suggesting that the phosphate species can be dissolved in solution during the irradiation. For comparison, the high-resolution XPS spectra of Ni 2p for the 0.5 wt % Ni<sub>2</sub>P/CdS NRs sample before and after photocatalytic reaction were examined (Figure S9). There are no obvious changes in Ni 2p<sub>3/2</sub> (855.8 eV) and Ni 2p<sub>1/2</sub> (874.0 eV) peaks. Furthermore, no metallic Ni was detected after visible light irradiation, suggesting that Ni<sub>2</sub>P does not decompose to produce metallic Ni during photocatalysis. The contents of Ni and P are 0.28 wt% and 2.34 wt% in Ni<sub>2</sub>P/CdS before irradiation, respectively (measured by ICP-AES). The P

content is high because of the existence of phosphate species. After 12 hours of irradiation, The contents of Ni and P are 0.38 wt% (corresponding to Ni<sub>2</sub>P 0.48 wt%) and 0.11 wt% (corresponding to Ni<sub>2</sub>P 0.51 wt%), respectively. And the mole ratio of Ni:P is 1.89:1 (nearly 2:1), further proving the product is Ni<sub>2</sub>P and the content of Ni<sub>2</sub>P is ~0.5 wt% in Ni<sub>2</sub>P/CdS. Moreover, the initial photocatalytic H<sub>2</sub> rate is relatively low, probably because of the existence of phosphate species bonded on the photocatalyst surface. The high resolution XPS spectrum of 10 wt% Ni<sub>2</sub>P/CdS samples were also performed (Figure S10). Compared to 0.5 wt% Ni<sub>2</sub>P/CdS, a new peak appeared in P 2p spectrum at 129.3 eV, which could be assigned P in Ni<sub>2</sub>P.<sup>53</sup> The 0.5 wt% Ni<sub>2</sub>P/CdS sample did not show this P peak, probably because of the low content of P in the photocatalyst, which can not be identified by XPS technique. In addition, SEM and TEM images of the 0.5 wt % Ni<sub>2</sub>P/CdS NRs sample after irradiation still show rod-like structures, which have nearly the same length and diameter as the samples before irradiation (Figure S11), and the HRTEM image of the sample after photocatalytic reaction also shows similar morphology with clear appearance of typical Ni<sub>2</sub>P and CdS lattice spacing (Figure S12). These results indicate that Ni<sub>2</sub>P/CdS NRs photocatalyst is highly robust in the present photosynthetic H<sub>2</sub> evolution system.

As compared with those reported in the literature, the aforementioned results show that the CdS NRs loaded with Ni<sub>2</sub>P have extraordinarily high catalytic performance for photocatalytic H<sub>2</sub> evolution under visible light irradiation. Very recently, a multi-component system by simply mixing Ni<sub>2</sub>P with CdS has been investigated for photocatalytic H<sub>2</sub> evolution in lactic acid solution.<sup>54</sup> However, the system showed much

lower catalytic activity (TON  $\sim$ 26,300 in 20 hours, TOF  $\sim$ 2,110 for Ni<sub>2</sub>P). In addition, the system has no good stability during photocatalysis. It was necessary to add additional CdS photoabsorber after only 20 hours of illumination, and hydrogen evolution rate significantly decreased during irradiation. Therefore, such high catalytic activity in our present work probably results from the formation of a well-designed CdS-Ni<sub>2</sub>P junction. The reductive side of water splitting in the system can be divided into several fundamental processes, including visible light absorption by the semiconductor, generation of electron-hole pairs, electron-hole pair separation, and transfer of electrons to water which results in the formation of H<sub>2</sub>. To identify the key factors responsible for the high H<sub>2</sub> evolution rate and quantum yield of Ni<sub>2</sub>P/CdS NRs, the light-absorption properties were measured and the results are shown in Figure 5a. The UV-vis DRS results show that the absorption edge of CdS is not shifted after Ni<sub>2</sub>P loading but the absorption level is enhanced, especially in the visible light region after 520 nm. Little change in the light absorption was observed, indicating that Ni<sub>2</sub>P was tightly deposited on the surface of CdS NRs instead of doping into the CdS lattice.

**The mechanism of Photocatalytic H<sub>2</sub> production.** Furthermore, organic electron acceptors were also used as indicators for the reducing power of Ni<sub>2</sub>P/CdS NRs. When methyl viologen dication (MV<sup>2+</sup>,  $3 \times 10^{-5}$  M) was added into an aqueous solution of Na<sub>2</sub>S (0.625 M), Na<sub>2</sub>SO<sub>3</sub> (0.875 M) and Ni<sub>2</sub>P/CdS NRs ( $8.3 \mu\text{g} \cdot \text{mL}^{-1}$ ) with 2 W LED flashlight irradiation in air, the solution color rapidly turned blue, indicating a fast electron transfer process and generation of viologen radical cations (MV<sup>•+</sup>).<sup>55</sup> After turning off the flashlight and exposing the solution to air for a long time, the color

remained blue and did not appreciably fade, even with shaking by hand in air (Supplementary Movie S4). When the solution containing  $MV^{2+}$  was irradiated with a 300 W Xe lamp ( $\lambda > 420$  nm), the radical product  $MV^{+\bullet}$  was quickly ( $< 5$  seconds) generated and its absorption intensity was saturated within one minute (Figure 5b), implying the strong reducing power of  $Ni_2P/CdS$  NRs. Since diquat ( $DQ^{2+}$ , N,N'-(1,3-propylene)-5,5'-dimethylbipyridine) has much higher reduction potential ( $-0.7$  V vs. NHE<sup>38</sup>) than  $MV^{2+}$ , the reduced form  $DQ^{+\bullet}$  is a more powerful reducing reagent than  $MV^{+\bullet}$ . Further experiments were done using a  $DQ^{2+}$  electron acceptor to replace  $MV^{2+}$ . Under visible light irradiation, the solution color rapidly changed to pink and the UV-Vis spectra show a new absorption band in the visible region as the typical absorption character of reduced  $DQ^{+\bullet}$  (Figure 5c).<sup>56</sup> The absorption intensity of  $DQ^{+\bullet}$  was also saturated within only one minute. The formation of reduced  $DQ^{+\bullet}$  indicates that the reducing ability of  $Ni_2P/CdS$  NRs corresponds to a potential more negative than  $-0.7$  V versus NHE,<sup>38</sup> and thus the excited state is sufficiently reducing for  $H^+$  reduction. The color changes of photocatalytic reaction solutions containing  $MV^{2+}$  or  $DQ^{2+}$  are shown in Figure 5d.

To further understand the reason for the drastically enhanced photocatalytic activity of  $Ni_2P/CdS$  NRs for  $H_2$  evolution as compared to  $CdS$  NRs, we have further characterized these samples using photoluminescence (PL) spectra and time-resolved photoluminescence (TRPL) spectra, which are able to reflect the transfer of photogenerated charge carriers. Figure 6a shows the PL data under an excitation wavelength of 405 nm, and two distinct emission bands at about 511 and 713 nm can

be observed, which is in agreement with the previous reports.<sup>57-58</sup> Also, these emissions were remarkably quenched upon loading Ni<sub>2</sub>P, attributing to the fast transfer of electrons from CdS NRs to Ni<sub>2</sub>P, which can suppress the electron-hole recombination and enhance the photocatalytic activity. Besides this, the PL intensity of 0.5 wt. % Ni<sub>2</sub>P/CdS NRs is lower than 10 wt. % Ni<sub>2</sub>P/CdS NRs, which is consistent with former H<sub>2</sub> evolution activity. The transfer of photogenerated charge carriers of these samples has also been confirmed by the TRPL spectra. As shown in Figure 6b, the TRPL data further indicated that the lifetime of Ni<sub>2</sub>P/CdS NRs is much shorter than that of CdS NRs, also indicating the effective charge transfer from CdS NRs to Ni<sub>2</sub>P. The decay curves were fitted with exponentials to obtain the decay time. The results showed the value of CdS NRs have two lifetimes which are 6.44 ns and 0.50 ns. The short decay time component is considered to be due to quasi-free excitons, while the long component is attributed to localized exciton recombination, which are caused by de-trapping of carriers.<sup>59</sup> The 0.5 wt. % Ni<sub>2</sub>P/CdS NRs and 10 wt. % Ni<sub>2</sub>P/CdS NRs only have one decay lifetime each, which are 0.34 ns and 0.45 ns, respectively. The long lifetime component disappeared compared with CdS NRs alone, which could be the main influence on hydrogen evolution. Photocatalyst with reduction cocatalyst materials are expected to have shorter lifetime due to the efficient charge transfer from photocatalyst to cocatalyst on the surface and suppression of the electron-hole recombination. The much decreased lifetime value of Ni<sub>2</sub>P/CdS NRs clearly indicates that Ni<sub>2</sub>P is an effective cocatalyst for the charge transfer. Furthermore, the photocurrent tests were performed and the result is shown in Figure S13. It is observed that Ni<sub>2</sub>P/CdS

sample exhibited a highly enhanced photocurrent than CdS itself under the same conditions, revealing the efficient charge transfer process in Ni<sub>2</sub>P/CdS.<sup>60-61</sup>

## Conclusion

In conclusion, a visible light-driven system using Ni<sub>2</sub>P as the cocatalyst to form an integrated nanostructure with CdS semiconductor nanorods for photocatalytic H<sub>2</sub> evolution was successfully developed. The reaction components in the system consist of materials made of earth-abundant elements only, which makes this system quite intriguing for conversion of solar energy to chemical fuels. Ni<sub>2</sub>P could highly promote electron-hole pair separation and subsequent reduction of protons to generate H<sub>2</sub>. The photocatalytic activity of Ni<sub>2</sub>P/CdS NRs is extremely high, with impressive TOF and TON numbers in pure water which are among the highest reported to date.

## Methods

**Materials.** All the chemicals, including cadmium chloride hemipentahydrate (CdCl<sub>2</sub> · 2.5H<sub>2</sub>O), cadmium diacetate dehydrate (Cd(OAc)<sub>2</sub> · 2H<sub>2</sub>O), thiourea (NH<sub>2</sub>CSNH<sub>2</sub>), ethylenediamine (C<sub>2</sub>H<sub>4</sub>(NH<sub>2</sub>)<sub>2</sub>), nickel nitrate hexahydrate (Ni(NO<sub>3</sub>)<sub>2</sub> · 6H<sub>2</sub>O), sodium sulfide nonahydrate (Na<sub>2</sub>S · 9H<sub>2</sub>O), and anhydrous sodium sulfate (Na<sub>2</sub>SO<sub>3</sub>), were all obtained from Aldrich and used without further purification.

Preparation of the CdS NRs and CdS NPs: CdS NRs were fabricated as in previous research<sup>47</sup>. 20.25 mmol CdCl<sub>2</sub> · 2.5H<sub>2</sub>O and 60.75 mmol NH<sub>2</sub>CSNH<sub>2</sub> were dispersed in 60 mL ethylenediamine and then transferred to a 100 mL Teflon-lined, stainless-steel

autoclave, which was later maintained at 160 °C for 48 h and then allowed to cool down to room temperature. The yellow precipitates were collected and washed with absolute ethanol and distilled water to remove the residues of organic solvent. The CdS NPs were synthesized using a method described in previous literature.<sup>51</sup>

Preparation of the Ni<sub>2</sub>P/CdS NRs, Ni<sub>2</sub>P/CdS NRs and Ni<sub>2</sub>P: To synthesize Ni<sub>2</sub>P/CdS NRs, 200 mg CdS NRs, a calculated amount of Ni(NO<sub>3</sub>)<sub>2</sub> · 6H<sub>2</sub>O and yellow phosphorus (1:5) were dispersed in ethylenediamine under stirring. Subsequently, the mixture was transferred to a 50 mL Teflon liner and was solvothermally treated at 140 °C for 12 h. After the autoclave was cooled to room temperature, the precipitates were collected and washed with benzene, ethanol, and distilled water three times each. The final products were dried in vacuum at 60 °C overnight. The weight percentages of Ni<sub>2</sub>P in the various composites produced were 0.25, 0.5, 1.0, 2.0, 10.0, and 80.0. For comparison, pure Ni<sub>2</sub>P without CdS NRs and 0.5 wt% Ni<sub>2</sub>P/CdS NPs was also synthesized by a similar solvothermal reaction.

**Photocatalytic hydrogen evolution.** The photocatalytic hydrogen evolution experiments were carried out in a 50 mL flask with stirring at ambient temperature using a 300 W Xe lamp equipped with a UV cut-off filter ( $\lambda > 420$  nm). 1.0 mg of the photocatalyst was dispersed in 20 mL of aqueous solution containing Na<sub>2</sub>S and Na<sub>2</sub>SO<sub>3</sub> as sacrificial reagents, and then the suspension was stirred and purged with nitrogen for 20 min to remove air. Then, 5 mL of nitrogen was removed from the flask, followed by injecting 5 mL of methane (760 Torr) to serve as the internal standard<sup>55</sup>. For lengthy irradiations, a 250 mL flask and 50 mL aqueous solution were used instead. Hydrogen

gas was measured by gas chromatography (SP-6890, nitrogen as a carrier gas) using a thermal conductivity detector (TCD). For each evaluation of hydrogen generation, 100  $\mu\text{L}$  of the headspace was injected into the GC and was quantified by a calibration plot to the internal  $\text{CH}_4$  standard. The hydrogen evolution rate was calculated based on the  $\text{Ni}_2\text{P}/\text{CdS}$  NRs photocatalyst.

Apparent quantum yields (A.Q.Y.,  $\phi$ ) defined by the following equation were measured using a 300 W Xe lamp with 450 nm ( $\pm 5$  nm) band-pass filter and an irradiatometer:

$$\begin{aligned} \text{A. Q. Y. (\%)} &= \frac{\text{number of reacted electrons}}{\text{number of incident photons}} \times 100\% \\ &= \frac{\text{number of evolved H}_2 \text{ molecules} \times 2}{\text{number of incident photons}} \times 100\% \end{aligned}$$

The power of the light was 0.051 J/s, corresponding to the number of incident photons was  $1.155 \cdot 10^{17}$  photons/s, which was measured by using an irradiatometer (FZ-A, Beijing Normal University Optical Instrument).

The turnover number (TON) and turnover frequency (TOF) were calculated by using the following equations:

$$\begin{aligned} \text{TON} &= \frac{\text{moles of evolved H}_2}{\text{moles of Ni}_2\text{P on photocatalyst}} \\ \text{TOF} &= \frac{\text{TON}}{\text{reaction time (hours)}} \end{aligned}$$

**Photoelectrochemical measurements.** Photoelectrochemical measurements were tested on a CHI 602E electrochemical work station (Chenhua Instrument, Shanghai, China) in a standard three-electrode system with the photocatalyst-coated FTO as the working electrode, Pt wire as the counter electrode, and an Ag/AgCl as a reference

electrode. 300 W Xenon lamp with a UV cut-off filter ( $\lambda > 420$  nm) was used as the light source. A 0.5 M  $\text{Na}_2\text{SO}_4$  solution was used as the electrolyte. The working electrodes were prepared by dropping a suspension (30  $\mu\text{L}$ ) made of  $\text{Ni}_2\text{P}/\text{CdS}$  and  $\text{CdS}$  (10 mg  $\text{Ni}_2\text{P}/\text{CdS}$  and  $\text{CdS}$  added into 50  $\mu\text{L}$  Nafion and 450  $\mu\text{L}$  ethanol mixed solution, respectively) onto the surface of a FTO plate. The working electrodes were dried at room temperature. The photoresponsive signals of the samples were measured under chopped light at 0.0 V.

**Characterization.** The powder X-ray diffraction (XRD) was measured by X-ray diffraction (XRD, D/max-TTR III) using graphite monochromatized  $\text{Cu K}\alpha$  radiation of 1.54178 Å, operating at 40 kV and 200 mA. The scanning rate was  $5^\circ \text{ min}^{-1}$  in  $2\theta$ . The scanning electron microscopy (SEM) measurements were conducted using a JSM-6700F. Transmission electron microscopy (TEM) images and energy-dispersive X-ray analysis (EDX) were obtained with a JEM-2011 electron microscope equipped with a Rontec EDX system. The morphologies of the samples were also determined by a high-resolution transmission electron microscope (HR-TEM, JEM-2010) equipped with an electron diffraction (ED) attachment with an acceleration voltage of 200 kV. X-ray photoelectron spectroscopy (XPS) data and the valence states of metal elements were obtained with an ESCALAB 250 instrument. UV-Vis diffuse reflection spectroscopy (DRS) was performed on a SOLID 3700 UV-Vis spectrometer. The BET surface area was evaluated by  $\text{N}_2$  adsorption in an automated gas sorption analyzer (Autosorb-iQ, Quantachrome instrument). The photoluminescence (PL) spectra for solid samples were investigated through Acton Sp2500 (Princeton Instruments) with Liquid nitrogen

cooled CCD. The Time-resolved photoluminescence (TRPL) spectra was performed on PicoHarp 300 (PicoQuant). ICP-AES results were measured by an Optima 7300 DV.

**Supporting Information Available.** Experimental details are available including Nitrogen adsorption-desorption isotherms, SEM images, HRTEM images, additional XPS data of CdS/Ni<sub>2</sub>P. This material is available free of charge via the Internet at <http://pubs.rsc.org>.

### Acknowledgements

This work was financially supported by NSFC (21271166, 21473170), the Fundamental Research Funds for the Central Universities (WK3430000001, WK2060140015, WK2060190026), the Program for New Century Excellent Talents in University (NCET), and the Thousand Young Talents Program. We appreciate the kind help from Prof. Xiaoyong Wang at Nanjing University for assistance with the photoluminescence (PL) spectra and the time-resolved photoluminescence (TRPL) spectra.

### References

- (1) Gray, H. B. *Nat. Chem.* **2009**, *1*, 7.
- (2) Lewis, N. S.; Nocera, D. G. *Proc. Natl. Acad. Sci. U. S. A.* **2006**, *103*, 15729-15735.
- (3) Alstrum-Acevedo, J. H.; Brennaman, M. K.; Meyer, T. J. *Inorg. Chem.* **2005**, *44*, 6802-6827.
- (4) Eckenhoff, W. T.; McNamara, W. R.; Du, P.; Eisenberg, R. *Biochim. Biophys. Acta, Bioenerg.* **2013**, *1827*, 958-973.
- (5) Nocera, D. G. *Acc. Chem. Res.* **2012**, *45*, 767-776.
- (6) Bard, A. J.; Fox, M. A. *Acc. Chem. Res.* **1995**, *28*, 141-145.

- (7) Han, Z.; Eisenberg, R. *Acc. Chem. Res.* **2014**, *47*, 2537-2544.
- (8) Wen, F.; Li, C. *Acc. Chem. Res.* **2013**, *46*, 2355-2364.
- (9) Du, P.; Eisenberg, R. *Energy Environ. Sci.* **2012**, *5*, 6012-6021.
- (10) Artero, V.; Chavarot-Kerlidou, M.; Fontecave, M. *Angew. Chem. Int. Ed.* **2011**, *50*, 7238-7266.
- (11) Tard, C.; Pickett, C. J. *Chem. Rev.* **2009**, *109*, 2245-2274.
- (12) Simmons, T. R.; Berggren, G.; Bacchi, M.; Fontecave, M.; Artero, V. *Coord. Chem. Rev.* **2014**, *270-271*, 127-150.
- (13) Mondal, B.; Sengupta, K.; Rana, A.; Mahammed, A.; Botoshansky, M.; Dey, S. G.; Gross, Z.; Dey, A. *Inorg. Chem.* **2013**, *52*, 3381-3387.
- (14) Quentel, F.; Passard, G.; Gloaguen, F. *Energy Environ. Sci.* **2012**, *5*, 7757-7761.
- (15) Bediako, D. K.; Lassalle-Kaiser, B.; Surendranath, Y.; Yano, J.; Yachandra, V. K.; Nocera, D. G. *J. Am. Chem. Soc.* **2012**, *134*, 6801-6809.
- (16) Chen, S.; Duan, J. J.; Ran, J. R.; Jaroniec, M.; Qiao, S. Z. *Energy Environ. Sci.* **2013**, *6*, 3693-3699.
- (17) Dinca, M.; Surendranath, Y.; Nocera, D. G. *Proc. Natl. Acad. Sci. U. S. A.* **2010**, *107*, 10337-10341.
- (18) Yu, X.; Hua, T.; Liu, X.; Yan, Z.; Xu, P.; Du, P. *ACS Appl. Mater. Interfaces* **2014**, *6*, 15395-15402.
- (19) Han, A.; Wu, H.; Sun, Z.; Jia, H.; Yan, Z.; Ma, H.; Liu, X.; Du, P. *ACS Appl. Mater. Interfaces* **2014**, *6*, 10929-10934.
- (20) Jiao, F.; Frei, H. *Angew. Chem., Int. Ed.* **2009**, *48*, 1841-1844.
- (21) Cobo, S.; Heidkamp, J.; Jacques, P. A.; Fize, J.; Fourmond, V.; Guetaz, L.; Jusselme, B.; Ivanova, V.; Dau, H.; Palacin, S.; Fontecave, M.; Artero, V. *Nat. Mater.* **2012**, *11*, 802-807.
- (22) Liang, Y.; Li, Y.; Wang, H.; Zhou, J.; Wang, J.; Regier, T.; Dai, H. *Nat. Mater.* **2011**, *10*, 780-786.
- (23) Hinnemann, B.; Moses, P. G.; Bonde, J.; Jørgensen, K. P.; Nielsen, J. H.; Horch, S.; Chorkendorff, I.; Nørskov, J. K. *J. Am. Chem. Soc.* **2005**, *127*, 5308-5309.
- (24) Jaramillo, T. F.; Jørgensen, K. P.; Bonde, J.; Nielsen, J. H.; Horch, S.; Chorkendorff, I. *Science* **2007**, *317*, 100-102.
- (25) Benck, J. D.; Chen, Z. B.; Kuritzky, L. Y.; Forman, A. J.; Jaramillo, T. F. *ACS Catal.* **2012**, *2*, 1916-1923.
- (26) Merki, D.; Hu, X. L. *Energy Environ. Sci.* **2011**, *4*, 3878-3888.
- (27) Vrubel, H.; Merki, D.; Hu, X. L. *Energy Environ. Sci.* **2012**, *5*, 6136-6144.
- (28) Voiry, D.; Yamaguchi, H.; Li, J. W.; Silva, R.; Alves, D. C. B.; Fujita, T.; Chen, M. W.; Asefa, T.; Shenoy, V. B.; Eda, G.; Chhowalla, M. *Nat. Mater.* **2013**, *12*, 850-855.
- (29) Baffert, C.; Artero, V.; Fontecave, M. *Inorg. Chem.* **2007**, *46*, 1817-1824.
- (30) McCrory, C. C. L.; Uyeda, C.; Peters, J. C. *J. Am. Chem. Soc.* **2012**, *134*, 3164-3170.
- (31) Utschig, L. M.; Silver, S. C.; Mulfort, K. L.; Tiede, D. M. *J. Am. Chem. Soc.* **2011**, *133*, 16334-16337.
- (32) Dubois, M. R.; Dubois, D. L. *Acc. Chem. Res.* **2009**, *42*, 1974-1982.

- (33) Helm, M. L.; Stewart, M. P.; Bullock, R. M.; DuBois, M. R.; DuBois, D. L. *Science* **2011**, *333*, 863-866.
- (34) McCormick, T. M.; Calitree, B. D.; Orchard, A.; Kraut, N. D.; Bright, F. V.; Detty, M. R.; Eisenberg, R. *J. Am. Chem. Soc.* **2010**, *132*, 15480-15483.
- (35) McLaughlin, M. P.; McCormick, T. M.; Eisenberg, R.; Holland, P. L. *Chem. Commun.* **2011**, *47*, 7989-7991.
- (36) McNamara, W. R.; Han, Z.; Alperin, P. J.; Brennessel, W. W.; Holland, P. L.; Eisenberg, R. *J. Am. Chem. Soc.* **2011**, *133*, 15368-15371.
- (37) Zong, X.; Yan, H.; Wu, G.; Ma, G.; Wen, F.; Wang, L.; Li, C. *J. Am. Chem. Soc.* **2008**, *130*, 7176-7177.
- (38) Han, Z.; Qiu, F.; Eisenberg, R.; Holland, P. L.; Krauss, T. D. *Science* **2012**, *338*, 1321-1324.
- (39) Li, Z.-J.; Li, X.-B.; Wang, J.-J.; Yu, S.; Li, C.-B.; Tung, C.-H.; Wu, L.-Z. *Energy Environ. Sci.* **2013**, *6*, 465-469.
- (40) Peng, T. Y.; Zhang, X. H.; Zeng, P.; Li, K.; Zhang, X. G.; Li, X. G. *J. Catal.* **2013**, *303*, 156-163.
- (41) Khan, Z.; Khannam, M.; Vinothkumar, N.; De, M.; Qureshi, M. *J. Mater. Chem.* **2012**, *22*, 12090-12095.
- (42) Yan, Z.; Yu, X.; Han, A.; Xu, P.; Du, P. *J. Phys. Chem. C* **2014**, *118*, 22896-22903.
- (43) Zhang, W.; Wang, Y.; Wang, Z.; Zhong, Z.; Xu, R. *Chem. Commun.* **2010**, *46*, 7631-7633.
- (44) Tongying, P.; Plashnitsa, V. V.; Petchsang, N.; Vietmeyer, F.; Ferraudi, G. J.; Krylova, G.; Kuno, M. *J. Phys. Chem. Lett.* **2012**, *3*, 3234-3240.
- (45) Wang, L.; Wei, H. W.; Fan, Y. J.; Gu, X.; Zhan, J. H. *J. Phys. Chem. C* **2009**, *113*, 14119-14125.
- (46) Yang, G. R.; Yan, W.; Zhang, Q.; Shen, S. H.; Ding, S. J. *Nanoscale* **2013**, *5*, 12432-12439.
- (47) Jang, J. S.; Joshi, U. A.; Lee, J. S. *J. Phys. Chem. C* **2007**, *111*, 13280-13287.
- (48) Abe, R.; Sayama, K.; Arakawa, H. *Chem. Phys. Lett.* **2003**, *371*, 360-364.
- (49) Kato, H.; Asakura, K.; Kudo, A. *J. Am. Chem. Soc.* **2003**, *125*, 3082-3089.
- (50) Chen, X. B.; Shen, S. H.; Guo, L. J.; Mao, S. S. *Chem. Rev.* **2010**, *110*, 6503-6570.
- (51) Yan, H.; Yang, J.; Ma, G.; Wu, G.; Zong, X.; Lei, Z.; Shi, J.; Li, C. *J. Catal.* **2009**, *266*, 165-168.
- (52) Wang, W.; Zhai, J.; Bai, F. *Chem. Phys. Lett.* **2002**, *366*, 165-169.
- (53) Zhang, S.; Zhang, S.; Song, L.; Wu, X.; Fang, S. *Mater. Res. Bull.* **2014**, *53*, 158-162.
- (54) Cao, S.; Chen, Y.; Wang, C. J.; He, P.; Fu, W. F. *Chem. Commun.* **2014**, *50*, 10427-10429.
- (55) Du, P.; Schneider, J.; Jarosz, P.; Zhang, J.; Brennessel, W. W.; Eisenberg, R. *J. Phys. Chem. B.* **2007**, *111*, 6887-6894.
- (56) Kung, J. W.; Baumann, S.; von Bergen, M.; Muller, M.; Hagedoorn, P. L.; Hagen, W. R.; Boll, M. *J. Am. Chem. Soc.* **2010**, *132*, 9850-9856.

- (57) Liu, S. Q.; Chen, Z.; Zhang, N.; Tang, Z. R.; Xu, Y. J. *J. Phys. Chem. C* **2013**, *117*, 8251-8261.
- (58) Xu, D.; Liu, Z. P.; Liang, J. B.; Qian, Y. T. *J. Phys. Chem. B* **2005**, *109*, 14344-14349.
- (59) Ma, G. H.; Tang, S. H.; Sun, W. X.; Shen, Z. X.; Huang, W. M.; Shi, J. L. *Phys. Lett. A* **2002**, *299*, 581-585.
- (60) Min, Y. L.; He, G. Q.; Xu, Q. J.; Chen, Y. C. *J. Mater. Chem. A* **2014**, *2*, 2578-2584.
- (61) Xie, Y. B. *Adv. Funct. Mater.* **2006**, *16*, 1823-1831.

## Figure Captions

**Figure 1. Integrated Ni<sub>2</sub>P/CdS NRs photocatalytic H<sub>2</sub> evolution system.** A schematic describing an artificial photocatalytic H<sub>2</sub> production system using CdS NRs as the photosensitizer and Ni<sub>2</sub>P as the cocatalyst.

**Figure 2. Photocatalytic activity of Ni<sub>2</sub>P/CdS NRs under different conditions.** (a) The rate of H<sub>2</sub> evolution on Ni<sub>2</sub>P/CdS NRs photocatalysts loaded with different amounts of Ni<sub>2</sub>P at room temperature under visible light ( $\lambda > 420$  nm). The system contains 1.0 mg photocatalyst, 0.75 M Na<sub>2</sub>S, and 1.05 M Na<sub>2</sub>SO<sub>3</sub> in 20 mL deionized water. (b) The rate of H<sub>2</sub> evolution on 0.5 wt % Ni<sub>2</sub>P/CdS NRs photocatalyst under different concentrations of the hole scavenger at room temperature under visible light ( $\lambda > 420$  nm): (A) 0.0625 M Na<sub>2</sub>S, 0.0875 M Na<sub>2</sub>SO<sub>3</sub>; (B) 0.25 M Na<sub>2</sub>S, 0.35 M Na<sub>2</sub>SO<sub>3</sub>; (C) 0.50 M Na<sub>2</sub>S, 0.70 M Na<sub>2</sub>SO<sub>3</sub>; (D) 0.75 M Na<sub>2</sub>S, 1.05 M Na<sub>2</sub>SO<sub>3</sub>; (E) 1.0 M Na<sub>2</sub>S, 1.4 M Na<sub>2</sub>SO<sub>3</sub>; (F) 1.25 M Na<sub>2</sub>S, 1.75 M Na<sub>2</sub>SO<sub>3</sub>; (G) 2.0 M Na<sub>2</sub>S, 2.8 M Na<sub>2</sub>SO<sub>3</sub>. The system contains 1.0 mg photocatalyst in 20 mL aqueous solution. Light source was Xe lamp (300 W) with a 420 nm long-pass cut filter.

**Figure 3. Photocatalytic H<sub>2</sub> evolution performance of Ni<sub>2</sub>P/CdS NRs.** (a) Long-term evolution of H<sub>2</sub> for 90 hours under visible light irradiation ( $\lambda > 420$  nm) using 0.5 wt % Ni<sub>2</sub>P/CdS NRs photocatalyst at room temperature. The system contains 1.0 mg photocatalyst, 1.25 M Na<sub>2</sub>S and 1.75 M Na<sub>2</sub>SO<sub>3</sub> in 50 mL deionized water. (b) Cycling runs for photocatalytic hydrogen evolution in the presence of 1.0 mg 0.5 wt % Ni<sub>2</sub>P/CdS NRs photocatalyst in a 50 mL aqueous solution containing 0.83 M Na<sub>2</sub>S and 1.16 M Na<sub>2</sub>SO<sub>3</sub> at room temperature. After every 2 hours, the produced H<sub>2</sub> was evacuated. (c) Comparison of photocatalytic H<sub>2</sub> evolution under N<sub>2</sub> and in air. Both systems contain the same components: 1.0 mg photocatalyst, 0.75 M Na<sub>2</sub>S and 1.05 M Na<sub>2</sub>SO<sub>3</sub> in 20 mL aqueous solution. (d) The time courses of H<sub>2</sub> evolution and apparent quantum yield on 0.5 wt% Ni<sub>2</sub>P/CdS NRs photocatalyst under monochromatic 450 nm light irradiation using 1.0 mg photocatalyst in a 20 mL aqueous solution containing 0.75 M Na<sub>2</sub>S and 1.05 M Na<sub>2</sub>SO<sub>3</sub>. The bars denote the apparent quantum yield. Generally, light source was Xe lamp (300 W) with a 420 nm long-pass cut filter.

**Figure 4. Characterization of the Ni<sub>2</sub>P/CdS NRs photocatalyst.** (a) SEM and (b) TEM image of 0.5 wt% Ni<sub>2</sub>P/CdS NRs. (c) EDX of 0.5 wt % Ni<sub>2</sub>P/CdS NRs and 10 wt % Ni<sub>2</sub>P/CdS NRs. (d) XRD patterns of Ni<sub>2</sub>P/CdS NRs photocatalysts containing different amount of Ni<sub>2</sub>P. (e) HRTEM image and (f) high-magnification HRTEM image of 0.5 wt % Ni<sub>2</sub>P/CdS NRs.

**Figure 5. UV-vis performance of Ni<sub>2</sub>P/CdS NRs under different condition.** (a) UV-vis diffuse reflectance spectra of CdS NRs (black line) and 0.5 wt % Ni<sub>2</sub>P/CdS NRs (red line). (b) UV-vis absorption spectra of 3 mL aqueous solution containing 0.5 wt % Ni<sub>2</sub>P/CdS NRs (8.3 μg·mL<sup>-1</sup>), MV<sup>2+</sup> (3×10<sup>-5</sup> M), 0.625 M Na<sub>2</sub>S and 0.875 M Na<sub>2</sub>SO<sub>3</sub> before irradiation (black line), and after irradiation (λ > 420 nm) for 60 s (red line). The solution was irradiated for 2 minutes, then the irradiation was stopped and the solution kept in air for 10 minutes (blue line). The insert image shows the time course of absorption changes at 603 nm under visible light irradiation (λ > 420 nm). Light source was Xe lamp (300 W) with a 420 nm long-pass cut filter. (c) UV-vis absorption spectra of 3 mL aqueous solution containing 0.5 wt % Ni<sub>2</sub>P/CdS NRs (8.3 μg·mL<sup>-1</sup>), DQ<sup>2+</sup> (3×10<sup>-5</sup> M), 0.625 M Na<sub>2</sub>S and 0.875 M Na<sub>2</sub>SO<sub>3</sub> before irradiation (black line), and after irradiation (λ > 420 nm) for 60 s under N<sub>2</sub> (red line). The solution was then exposed to air for 90 min (blue line). The difference of red and black spectra gives the absorption spectrum of the reduced DQ<sup>2+</sup> (dark cyan)<sup>56</sup>. The insert image shows the time course of absorption changes at 385 nm under visible light (λ > 420 nm). Light source was Xe lamp (300 W) with a 420 nm long-pass cut filter. (d) The color change images of the reaction system in a 3 mL aqueous solution containing 0.5 wt % Ni<sub>2</sub>P/CdS NRs (8.3 μg·mL<sup>-1</sup>), MV<sup>2+</sup> or DQ<sup>2+</sup> (3×10<sup>-5</sup> M), 0.625 M Na<sub>2</sub>S and 0.875 M Na<sub>2</sub>SO<sub>3</sub>. Top left: before irradiation (MV<sup>2+</sup>). Top middle: after irradiation (MV<sup>2+</sup>). Top right: exposed to air for 10 minutes (MV<sup>2+</sup>). Bottom left: before irradiation (DQ<sup>2+</sup>). Bottom middle: after irradiation (DQ<sup>2+</sup>). Bottom right: exposed to air for 2 minutes (DQ<sup>2+</sup>).

**Figure 6. Spectra performance of the Ni<sub>2</sub>P/CdS NRs photocatalyst.** (a) Photoluminescence spectra of CdS NRs at room temperature, pure CdS NRs, 0.5% Ni<sub>2</sub>P/CdS NRs, and 10% Ni<sub>2</sub>P/CdS NRs with an excitation wavelength of 405 nm. (b) Time-resolved photoluminescence (TRPL) spectra of pure CdS NRs, 0.5% Ni<sub>2</sub>P/CdS NRs, and 10% Ni<sub>2</sub>P/CdS NRs with an excitation wavelength of 405 nm.

Figure 1

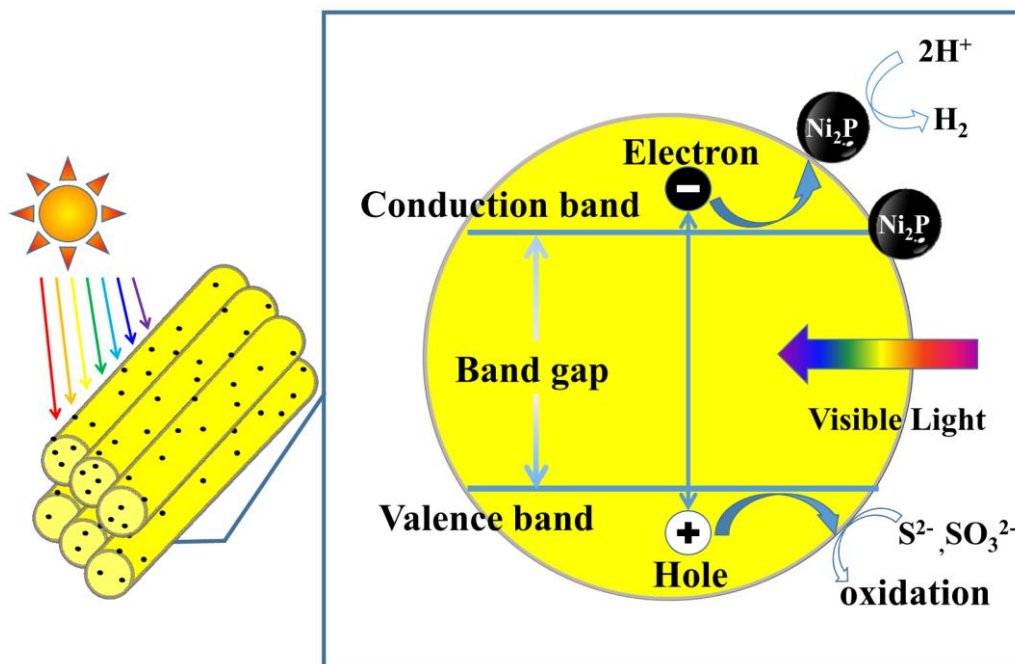


Figure 2

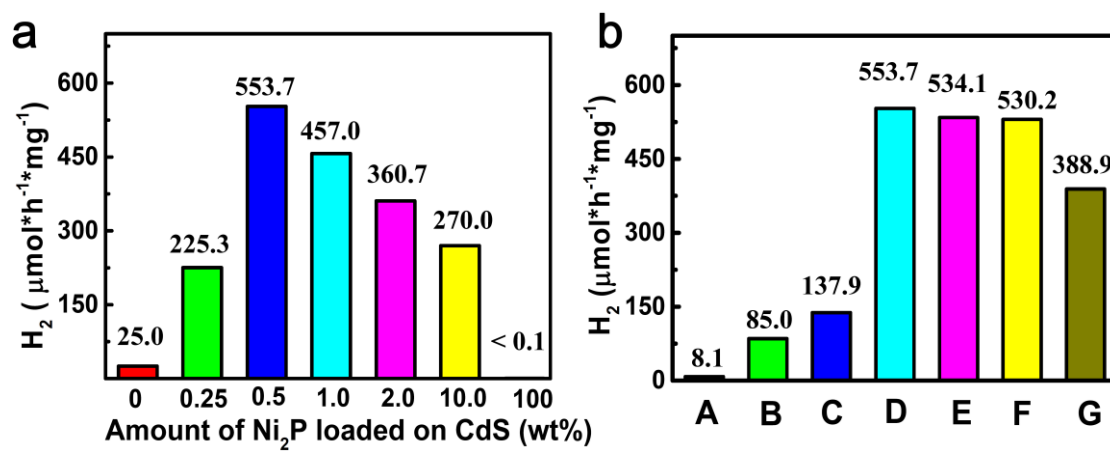


Figure 3

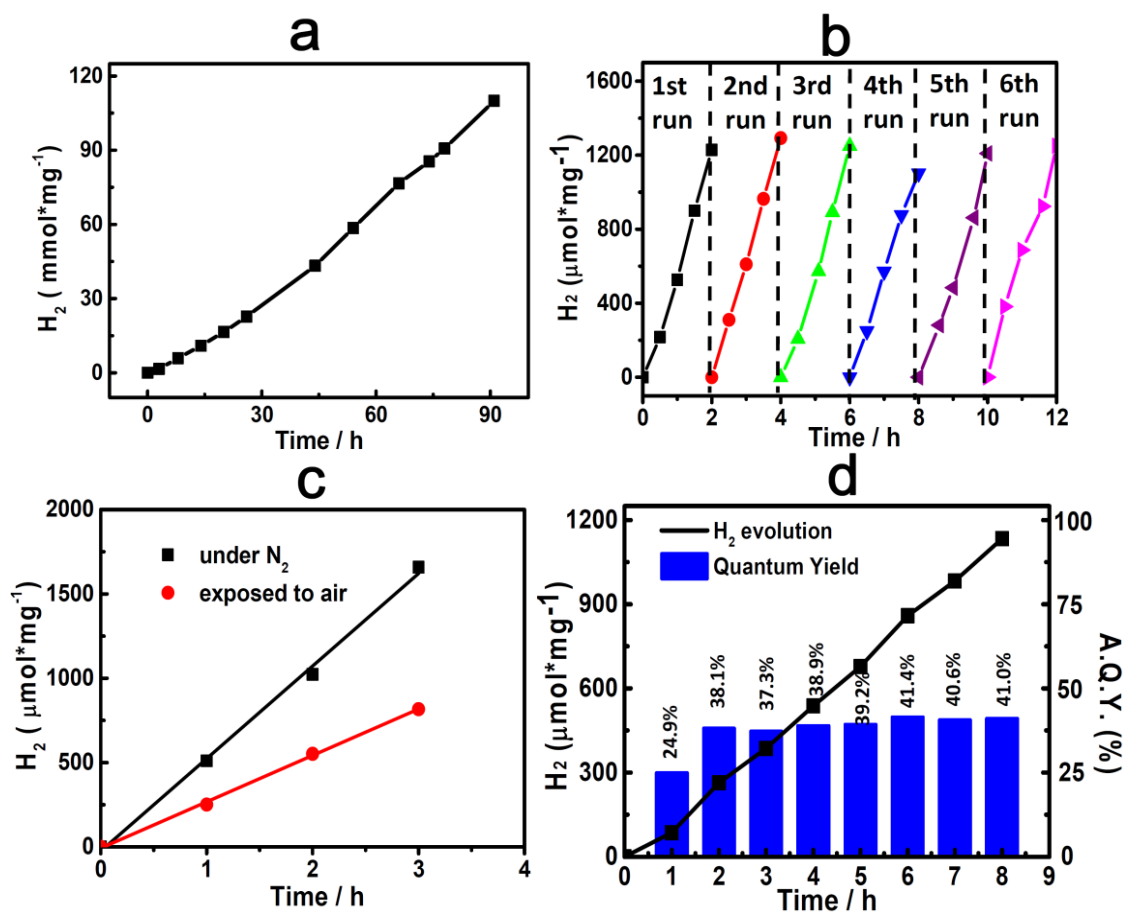


Figure 4

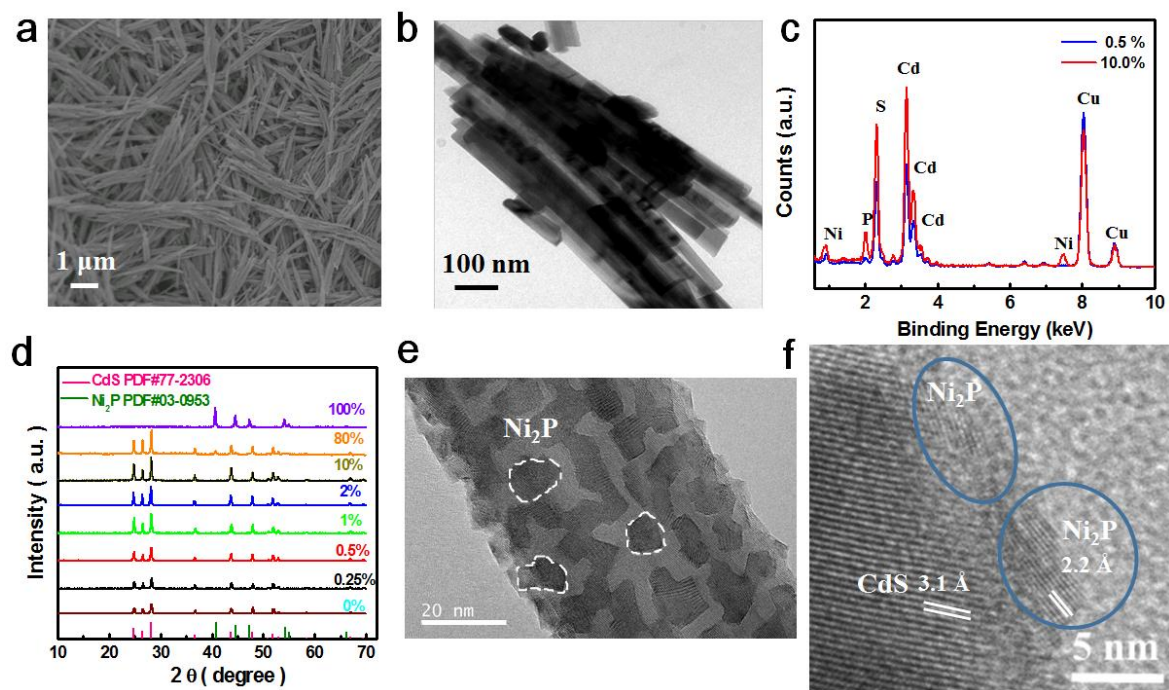


Figure 5

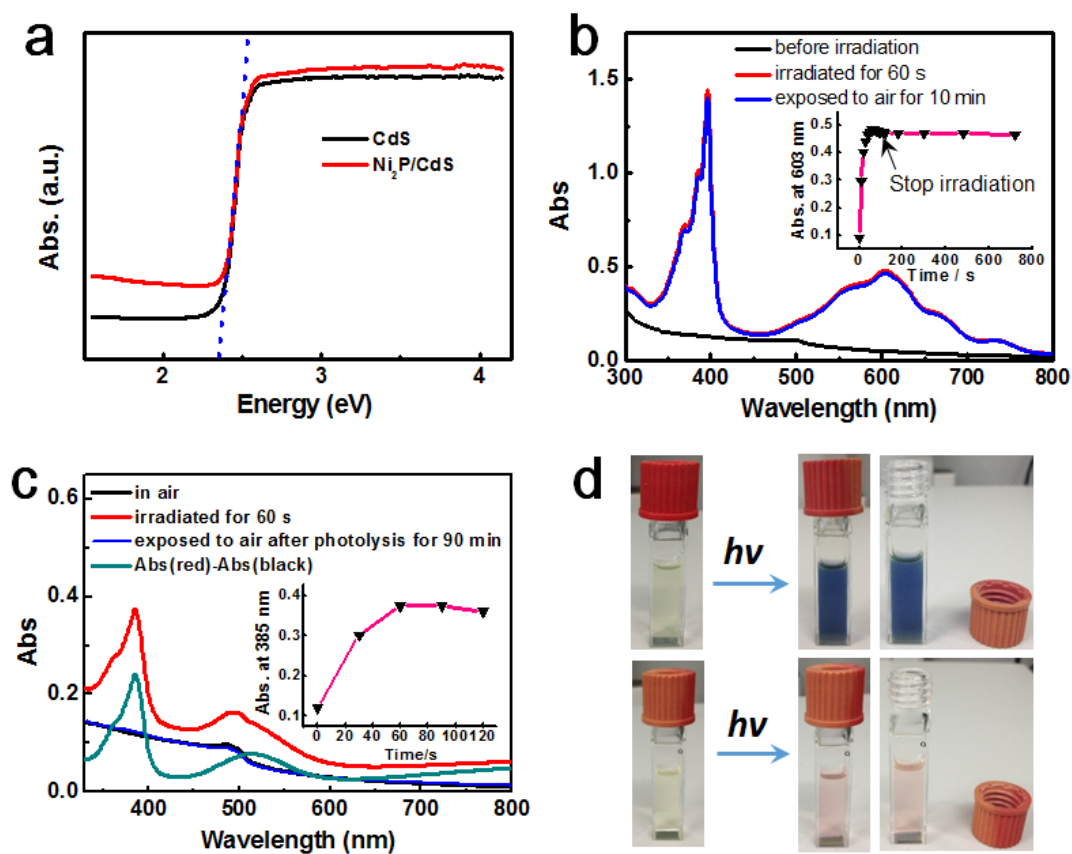
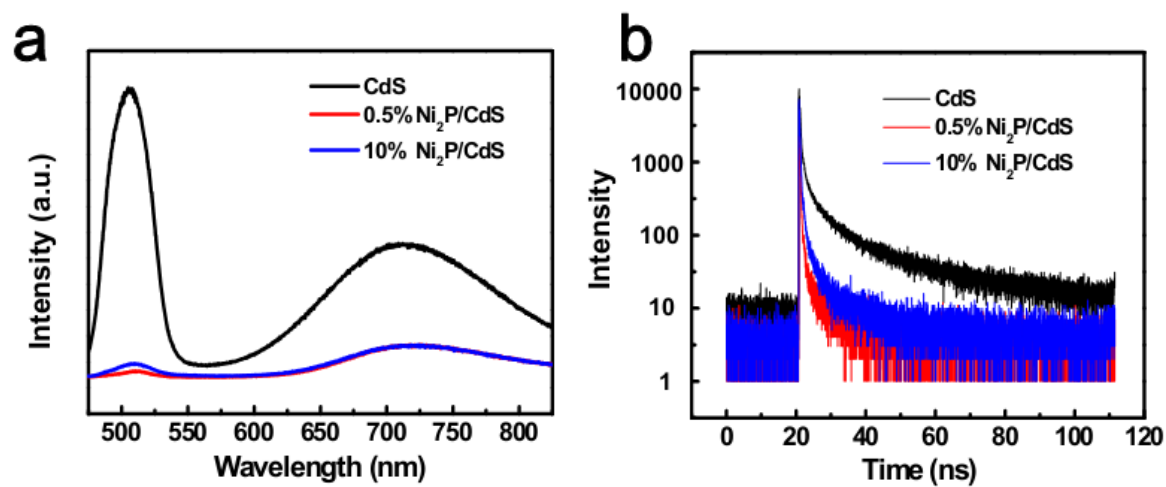


Figure 6



## Table of Contents

